NMR Study of Lithium Dynamics and Molecular Motions in a Diethylamine−Molybdenum Disulfide Intercalation Compound

Antonio Carlos Bloise, José Pedro Donoso,* Claudio José Magon, José Schneider, and Horácio Panepucci

Instituto de Física de São Carlos, Universidade de São Paulo, P.O. Box 369, 13560-970 São Carlos, S.P. Brazil

Eglantina Benavente

Departamento de Química, Universidad Tecnológica Metropolitana, Av. J.P. Alessandri 1242, Santiago, Chile

Víctor Sanchez, Maria Angélica Santa Ana, and Guillermo González

Departamento de Química, Facultad de Ciencias, Universidad de Chile, P.O. Box 653, Santiago, Chile

Received: July 24, 2001; In Final Form: July 26, 2002

Measurements of the ^{13}C, ^{7}Li, and ^{1}H nuclear magnetic resonance (NMR) of the nanocomposite formed by the intercalation of lithium and diethylamine in molybdenum disulfide, $Li_{0.1}MoS_2[(C_2H_5)_2NH]_{0.2}$, are reported. The strong Li−Li dipolar interaction strength, calculated from the ^{7}Li NMR decoupling data, suggests the formation of lithium clusters. The dimensional restriction of the available space between the host layers supports a hypothesis that is based on the formation of Li_3 clusters stabilized by amine ligands. The lithium relaxation is mainly due to the interaction between the quadrupolar moment of the ^{7}Li nuclei and the fluctuating electric field gradient at the site of the nucleus, produced by the surrounding charge distribution. The dynamical parameters obtained from the ^{7}Li temperature dependence of the spin−lattice relaxation indicate a high lithium mobility, which is attributed to the fast exchange motion of the lithium ions between the coordination sites within each Li_3 aggregate. The ^{1}H line shape and relaxation data support the proposed structural model for the lithium−diethylamine cluster. Numerical analysis of the ^{1}H line shape indicates that the intercluster dipole−dipole interactions are responsible for most of the spectral broadening. ^{1}H spin−lattice relaxation is mainly governed by hydrogen nuclei in the less-mobile CH_2 and in the fast-relaxing CH_3 groups in the diethylamine molecule.

I. Introduction

Intercalation compounds of the group 4−6 transition-metal dichalcogenides (MX_2) have been widely studied during the last two decades, especially because of their importance as materials for electrodes in solid-state batteries.[1−3] The interest in these materials arises not only from their potential applications but also from the physics associated with the electronic band structure of the host and the mixed ionic−electronic conducting properties of the products. The most relevant structural characteristic of these compounds is their laminar nature. MS_2 slabs are formed by relatively strong ionic−covalent bonds between the metal and the chalcogenide. In the solid state, the MS_2 layers are held together by relatively weak electrostatic forces generating the interlaminar spaces (called van der Waals gaps), into which the metal ions and other chemical species can be intercalated. In lithium-intercalated derivatives, the ionic transport is related to the appreciable mobility of lithium ions in the 2D interlayer spaces, whereas the electronic transport is mainly related to the transition-metal d electrons. The structural, electrical, and magnetic properties of these intercalation compounds have been reviewed.[3−5]

Molybdenum disulfide is a diamagnetic semiconductor with a modulated structure consisting of S−Mo−S layers. The electronic and magnetic properties of MoS_2 can be altered significantly by the insertion of alkali ions into the van der Waals gaps.[1,3,6] Upon lithium intercalation, the local coordination of the Mo centers in the host changes from trigonal prismatic (2H−MoS_2) to distorted octahedral (1T-MoS_2). MoS_2−amine compounds are especially interesting for the design of fast ionic conductors with molecular architectures intercalated between the layers, which allows for the enhancement and control of the transport properties. Substantial progress has been made during the past decade in the intercalation of molecules and polymers into the interlayer space of molybdenum disulfide,[3] namely, polyaniline,[7] polypyrrole,[8] nitro and amino biothiophenes,[9] hydrated alkali metal,[10] polymer electrolytes based on poly(ethylene oxide),[11,12] phenanthroline,[13] and ammonia.[14] Recently, the intercalation of dialkylamine into MoS_2 was reported.[15]

Nuclear magnetic resonance (NMR) is a well-known experimental technique that is used to study the ionic and molecular dynamics of nanostructured materials. In the past decade, it has been extensively used to study lithium mobility in intercalated compounds[16,17] as well as to understand the dynamics of molecules and polymers accommodated in layered materials[18−23]

* Corresponding author. E-mail: donoso@if.sc.usp.br. Fax: +55 16 271 3616.

10.1021/jp012839m CCC: $22.00
Published on Web 10/16/2002

or in relatively large spaces in host crystalline structures.[24−26] In this paper, we report a carbon (^{13}C), proton (^{1}H), and lithium (^{7}Li) NMR investigation of the layered organic−inorganic nanocomposite obtained from the co-intercalation of diethylamine and lithium into molybdenum disulfide, $Li_{0.1}MoS_2[(C_2H_5)_2NH]_{0.2}$ (hereafter denoted $Li_{0.1}MoS_2$[d-eth]$_{0.2}$). The NMR decoupling technique was used to discriminate between the different lithium interactions (Li−Li and Li−H) and to provide detailed quantitative information on the lithium cluster structure in the investigated nanocomposite. Results of the NMR line shapes and spin−lattice relaxation measurements are interpreted on the basis of a proposed structural model for the lithium−amine aggregate, giving relevant information on the structure and dynamics of the lithium ions and amine groups.

II. Experimental Section

Intercalation of Diethylamine into MoS_2. Amine was added to a suspension of exfoliated MoS_2 prepared by treating Li_xMoS_2 ($x = 0.9-1.2$) with deionized deaerated water. The suspension was stirred for 24 h at room temperature, and the solid product was separated, washed, dried under vacuum, and stored under an argon atmosphere. Li_xMoS_2 was prepared by treating a suspension of MoS_2 with a solution of 1.6 M butyllithium in *n*-hexane for 48 h at room temperature.[15,27] When dealing with small amounts of the product, microwave irradiation of the reaction mixture may be used as an alternative method.[28] The product was then washed with *n*-hexane and dried and stored inside a glovebox under an argon atmosphere. Careful washing of the product with *n*-hexane guarantees that the amine is strongly retained by MoS_2.

The amine−Li_xMoS_2 intercalation compound was characterized by determining its conformation by combustion analysis for C, H, N, and S (SISONS EA-1108); atomic absorption spectroscopy for Li (UNICAM 929, 670.8 nm); and TG/DTA simultaneous thermal analysis (Netzsch STA 409C, 10−900 °C, 10 °C/min, Ar atmosphere). Structural analyses as well as purity tests of the obtained phases were performed by powder X-ray diffraction analysis (Siemens D-5000 with Cu Kα radiation). The results of the analysis for $Li_{0.1}MoS_2(C_4H_{11}N)_{0.2}$ are the following: C 5.57% (calculated 5.85%); H 1.33 (1.34); N 1.99 (1.70); Li 0.41 (0.39). Elemental analysis as well as IR spectra shows the absence of water in the product. Thermal analysis corroborates the stability of the intercalate as well as the composition of the product. FTIR absorption in the range 3500−3300 cm^{-1}, assigned to the N−H stretching frequency, and the absence of the NH^+ bending modes in the range 1635−1380 cm^{-1}, assigned to alkylammonium compounds, indicate that the chemical species intercalated into MoS_2 corresponds to the free amine and not to the diethylammonium ion.

The mixed ionic−electronic conducting nature of the product was determined by measuring both the electrical and ionic conductivity by independent methods. Electrical conductivity was measured by electrochemical impedance spectroscopy for a sample pressed between ion-blocking gold electrodes. Ionic conductivity was obtained by galvanostatic relaxation techniques using the symmetric cell Li/Li salt solution/sample/Li salt solution/Li. The electrical and ionic conductivities at 25 °C are 0.25 S/cm and 8×10^{-7} S/cm, respectively.

For the intercalation compound Li_xMoS_2, the charge transfer from lithium to the matrix appears to be only partial, especially at high lithium concentrations.[3,29] However, when lithium is co-intercalated with a donor such as dietylamine, the electron transfer should be complete. Indeed, a solid-state high-resolution ^{7}Li NMR experiment, performed at room temperature, indicates that there is no displacement of the chemical shift in the lithium−amine−MoS_2 intercalate with respect to that in the aqueous solution of LiCl.

The existence of paramagnetic centers (or impurities) in the amine−Li_xMoS_2 intercalation compounds was evidenced by X-band electron paramagnetic resonance (EPR) measurements carried out at room temperature in a Bruker E-580 spectrometer. Two compounds ($x = 0.1$ and 0.7) were studied, and the intensity of the EPR absorption line seems to be strongly dependent on the lithium content of the samples (i.e., the line intensity increases with the lithium concentration). For both samples, two superimposed absorption lines were observed, having similar g factors ($g \approx 2$) and line widths of about 10 and 100 G ($x = 0.1$) and 2 and 100 G ($x = 0.7$), respectively. A sample with $x = 0.1$, which was used throughout this work, presented a weak EPR signal (signal-to-noise ratio around 2), indicating a low concentration of paramagnetic centers. Such a weak EPR feature has been attributed to unpaired electrons stabilized in the sulfur chains.[30]

Nuclear Magnetic Resonance. Proton (^{1}H) NMR line-width and spin−lattice relaxation-time (T_1) measurements were carried out on a pulsed NMR spectrometer operating at 36 MHz equipped with a TECMAG NMR kit. Spin−lattice relaxation times were determined using the standard saturation−recovery method and a $\pi/2$ pulse length of about 2 μs in the temperature range of 93−353 K. The ^{7}Li and ^{13}C NMR measurements were performed on a Varian 400-MHz INOVA spectrometer. The ^{7}Li spectrum and relaxation-time measurements were performed at 155.4 MHz using a wide-line Varian probe in the temperature range of 140−353 K. The ^{7}Li line shape was obtained from the Fourier transform of the decaying part of the quadrupolar echo ($t > 2\tau$) generated by the sequence $(\pi/2)_x - \tau - (\pi/2)_y$ using $\tau \approx 40$ μs, 16 accumulations, nonselective $\pi/2$ pulses of 2 μs, and phase cycling for the suppression of spurious signals.[31] Additional tests were done with a conventional Hahn-echo sequence, giving comparable results. ^{7}Li spin−lattice relaxation times were determined by applying the saturation−recovery method, $\pi/2 - \tau - \pi/2$, with a pulse spacing of up to $8T_1$ for each temperature and four accumulations. The high-resolution ^{13}C NMR spectra were obtained at 100.6 MHz in a magic-angle spinning (MAS) multinuclear probe (spinning frequency of 4.5 and 5.5 kHz) using cross polarization (CP) and proton decoupling. A relaxation delay of 5 s, a $\pi/2$ pulse length of 3.5 μs, and a contact time of 100 μs were used. The ^{7}Li MAS NMR spectra were obtained at 155.4 MHz by using a spinning frequency of 4.7 kHz, a relaxation delay of 30 s, and a $\pi/2$ pulse length of 3 μs. The heteronuclear dipolar interactions (mainly Li−H) were removed from the ^{7}Li spectra by the use of the decoupling technique, performed at 170 K under a magnetic field of 9.4 T, by exciting the ^{1}H nuclear system with the Larmor frequency of 400 MHz.

III. Results and Discussion

X-ray Diffraction. Figure 1 shows the powder X-ray diffraction pattern (XRD) of the molybdenum disulfide−diethylamine nanocomposite Li_xMoS_2[d-eth] compared with that of pristine MoS_2, which has a basal spacing of 6.14 Å. The XRD pattern of the nanocomposite displays the typical [00l] reflections of a relatively ordered laminar solid, indicating that the product is a pure-phase compound with an interlaminar distance of 9.8 Å. The increase of the MoS_2 interlaminar distance, $\Delta c = 3.66$ Å, agrees with those reported previously for $Li_{0.11}MoS_2$[d-eth]$_{0.42}$ ($\Delta c = 3.74$ Å).[15]

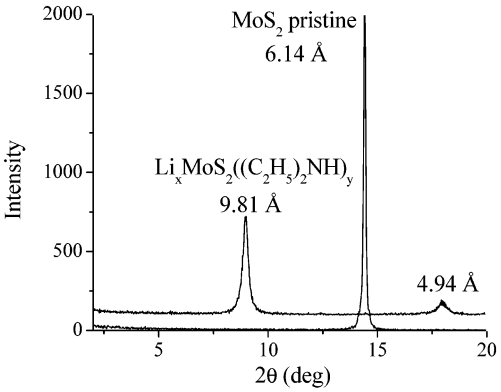

Figure 1. XRD patterns of pristine molybdenum disulfide and its diethylamine intercalation compound, Li_xMoS_2 [d-eth].

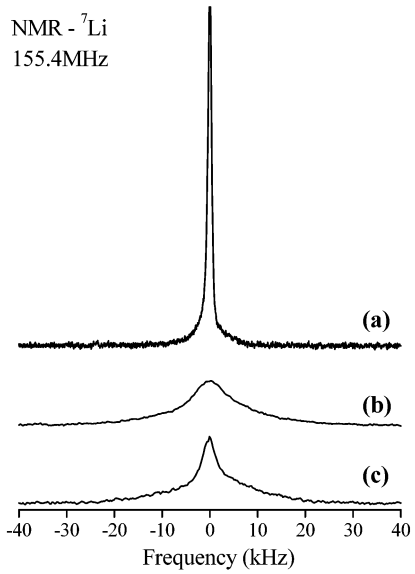

Figure 2. Comparison of the ^{7}Li NMR spectra of $Li_{0.1}MoS_2$ [d-eth]$_{0.2}$. (a) Motional-narrowed spectrum recorded at 263 K. Rigid-lattice spectrum recorded at 173 K without (b) and with (c) ^{1}H decoupling.

^{13}C NMR Spectra. The room-temperature ^{13}C CP/MAS NMR spectrum of solid $Li_{0.1}MoS_2$[d-eth]$_{0.2}$ shows intense peaks at 44.6 and 14.3 ppm, which are attributed to the diethylamine molecule, $CH_3-CH_2-NH-CH_2-CH_3$. By using standard software,[32] the spectrum simulation shows that the chemical shifts associated with the CH_2 and CH_3 groups are 44.1 and 15.3 ppm relative to TMS, respectively, in good agreement with the observed values.

^{7}Li NMR Spectra. The NMR powder spectrum of a nucleus with $I = {}^3/_2$ consists, up to first order in the quadrupolar perturbation, of a central line associated with the ${}^1/_2 \leftrightarrow -{}^1/_2$ transition and a symmetric pattern due to the ${}^3/_2 \leftrightarrow {}^1/_2$ and $-{}^1/_2 \leftrightarrow -{}^3/_2$ transitions.[33] However, the measured ^{7}Li spectra of $Li_{0.1}MoS_2$[d-eth]$_{0.2}$ at $T < 180$ K show a line shape consisting of a relatively narrow central line superimposed on a broad baseline, as can be seen in Figure 2b for $T = 173$ K. Such a spectrum can be simulated by a superposition of two Gaussian line shapes whose full width at half-height values are 8.5 ± 0.5 kHz and 30 ± 2 kHz. Above 190 K, the central resonance and the baseline narrow continuously upon increasing temperature as the shape of these lines changes from Gaussian to Lorentzian (Figure 2a).

To understand the nature of the broad component observed in the low-temperature spectra, two aspects should be considered. First, it is apparent that the peaks associated with the $\pm{}^3/_2 \leftrightarrow \pm{}^1/_2$ satellite transitions are not resolved in the measured ^{7}Li spectra. We point out that this situation is rather common in systems where the neighboring structure of the quadrupolar nuclei is distorted because of defects or disorder. Because, to first order, the satellite splitting is dependent on the electric field gradient, the distribution of the quadrupolar coupling constants produced by disorder may smear out the satellites.[34] Such a situation is certainly expected in this compound, and the observed broad baseline may indeed be attributed to quadrupolar effects. Second, it should be noted that the broad component is slightly asymmetric with respect to the central peak. This fact indicates that a contribution to the observed spectrum may arise from nonquadrupolar effects, such as the presence of ^{7}Li nuclei in different environments. This possibility will be further discussed during the analysis of the ^{7}Li relaxation.

TABLE 1: ^{7}Li and ^{1}H NMR Line Widths and Second Moments[a]

sample	^{7}Li line width (kHz)	^{7}Li−{^{1}H} line width (kHz)	line width reduction (%)	M_2(Li−Li) (G^2)
$Li_{0.1}MoS_2$[d-eth]$_{0.2}$	8.5	4.0	50	1.1
$Li_{0.1}MoS_2$[PEO]$_{0.5}$	8.0	0.9	90	0.05
PEO_8LiClO_4	6.4	0.5	90	0.02

[a] Line width of the ^{7}Li central line without ^{1}H decoupling (first column) and line width (second column) and second moment (fourth column) of the residual ^{7}Li central line after ^{1}H decoupling of (a) the studied nanocomposite formed by molybdenum disulfide and diethylamine, $Li_{0.1}MoS_2$[d-eth], (b) the intercalation compound $Li_{0.1}MoS_2$[PEO]$_{0.5}$ (from ref 35), and (c) the polymer electrolyte PEO_8LiClO_4 (from refs 36 and 37), where PEO is poly(ethylene oxide). The measurement temperature is 170 K.

For a nuclear spin of $I = {}^3/_2$, such as that for ^{7}Li, the central transition line width is primarily determined by dipole−dipole couplings.[16,22] In the nanocomposite $Li_{0.1}MoS_2$[d-eth]$_{0.2}$, the ^{7}Li central line is, to first order, broadened by homo- and heteronuclear dipolar contributions. The stable isotopes with nonzero nuclear spin (e.g., ^{14}N, ^{13}C, ^{95}Mo, and ^{33}S) have either a small magnetogyric ratio or a low natural abundance; therefore, it can be assumed that the main contributions to the observed lithium line width are the Li−Li and Li−H interactions.

The hetero- and homonuclear dipolar contributions to the ^{7}Li central line were determined by means of the high-power proton decoupling technique. Figure 2c shows the ^{7}Li−{^{1}H} decoupled spectra at 173 K, where the reduction of the line width of the central line can be observed without any noticeable effect on the broad base component. Table 1 summarizes the reduction of the ^{7}Li central line width after the proton decoupling. For the nanocomposite $Li_{0.1}MoS_2$[d-eth]$_{0.2}$, a reduction of about 50% was observed at 170 K. The analysis of the ^{7}Li−{^{1}H} decoupled central line, assuming a Gaussian shape, leads to a residual line width value of 4.0 ± 0.5 kHz (2.4 G) or a residual second moment M_2(Li−Li) ≈ 1.1 G^2. Such a residual line width is surprisingly large if compared to the values observed in the products of the intercalation of poly(ethylene oxide) in molybdenum disulfide, $Li_{0.1}MoS_2$[PEO]$_{0.5}$, where the proton decoupling causes a line width reduction of about 90%, as shown in Table 1.[35] A line width reduction of about 90% has also been reported for PEO/$LiClO_4$ and PPO/$LiClO_4$, where the lithium salt is practically dissolved into the polymeric matrix.[36,37]

Some hypotheses can be established to explain the strong Li−Li interaction observed in the investigated nanocomposite. On the basis of the assumption that the lithium ions occupy selected sites in the van der Waals gap, two remarks can be made. First, we point out that the experimental lithium second

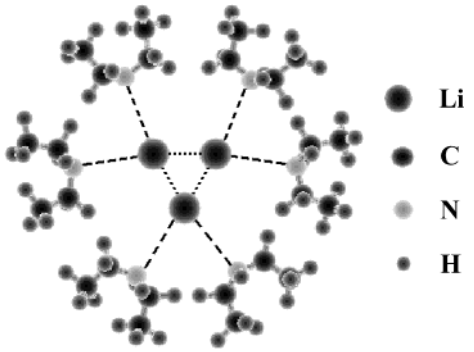

Figure 3. Structural model proposed for the lithium and diethylamine cluster, $Li_3[C_4H_{10}NH]_6$, formed by self-assembling by co-intercalation into molybdenum disulfide. The cluster has the shape of a thin disk of about a 15-Å diameter and a 3.9-Å width.

moment, M_2(Li−Li) ≈ 1.1 G^2, is not consistent with a homogeneous distribution of lithium in the sample. Indeed, considering the lithium content of 0.1 mol Li/mol MoS_2 and assuming that the lithium ions are located in a unique interlaminar surface, the average distance between neighboring ions would be around 7 Å. Because the second moment is proportional to the inverse of the sixth power of the internuclear distance, this result implies a very small second moment, M_2(Li−Li) ≈ 2×10^{-3} G^2. Such a small dipolar line width is comparable to those of other intercalation compounds such as $Li_{0.1}MoS_2[PEO]_{0.5}$, where M_2(Li−Li) is about 0.05 G^2 (Table 1) and where no lithium aggregation was observed. Therefore, in the amine intercalate discussed here, the formation of aggregates is evident.

Second, lithium's tendency to form aggregates is widely known, and many deltahedral clusters, such as the Li_4 tetrahedron in methyllithium, have been indeed described.[38−40] In the present case, the dimensional restrictions of the available space between host layers reinforce a hypothesis based on the formation of a triangular Li_3 species stabilized by amine ligands. After an examination of the known lithium cluster structures, the structural model of the intercalated lithium−amine complex was found to be that shown in Figure 3. The observed Li−Li second moment points to a Li−Li distance of about 2.8 Å, which is consistent with the expected value for a Li_3 cluster.[38] The second moment of the observed line shape, 4.8 G^2 (line width of 8.5 kHz), reduces to 1.1 G^2 (4 kHz) after ^{1}H decoupling. The second-moment reduction of 3.7 G^2 is due to the dipolar interaction between lithium nuclei in the cluster and amine hydrogen nuclei. This second moment contribution can be calculated from first principles on the basis of the spatial coordinates of the atoms of the proposed lithium−amine complex. Following this analysis, an internuclear distance from lithium to hydrogen belonging to the NH group of about 3.8 Å is inferred from the proposed complex model, leading to a value of 3.2 G^2, in good agreement with the measured Li−H second moment. On the basis of these data, a lithium−nitrogen distance of 3.7 Å is estimated. However, it is relatively large to correspond to formal Li−N bonds. Indeed, amine nitrogen atoms are forming a "coordination cage" that plays an important role in the stabilization of the positively charged trilithium cluster. Such large Li−N distances could be a result of the interplay between the charge of the Li cluster and the steric hindrance among the amine alkyl chains under 2D confinement. This issue remains under investigation.

Figure 4 shows the temperature dependence of the ^{7}Li central transition line width in $Li_{0.1}MoS_2$[d-eth]$_{0.2}$. The observed line-narrowing onset at 185 K arises from the motions of the Li^+ ions. In the case of a quadrupolar nuclei such as ^{7}Li, motional narrowing of the central transition begins when the rate of fluctuations of the local dipolar fields is comparable to the rigid-lattice line width. Quantitatively, the condition for narrowing can be expressed as $(\gamma M_2)^{1/2}\tau \ll 1$, where τ is the lithium motional correlation time and M_2 is the total lithium rigid-lattice second moment expressed in magnetic field units. Using $M_2 =$ 4.8 G^2, which corresponds to a measured rigid-lattice line width of about 8.5 kHz (Figure 4), the correlation time in the narrowed region must be $\tau \ll 4.4 \times 10^{-5}$ s.

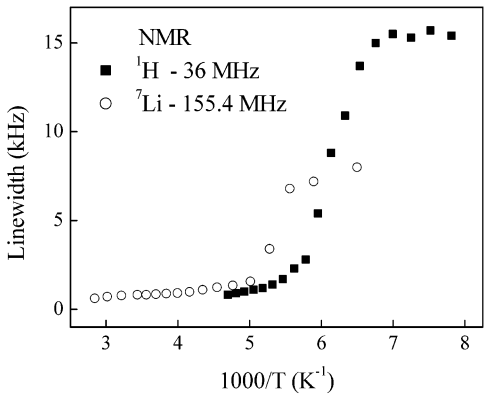

Figure 4. Temperature dependence of the line width of the ^{7}Li central transition and ^{1}H narrow line in $Li_{0.1}MoS_2$ [d-eth]$_{0.2}$.

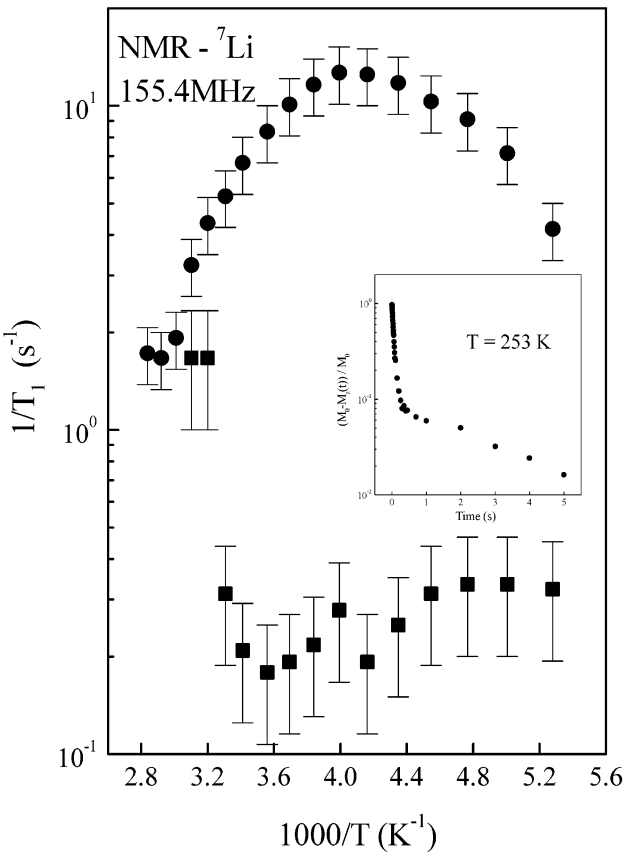

Figure 5. Temperature dependence of the fast (T_{1a}^{-1}) (●) and slow (T_{1b}^{-1}) (■) spin−lattice relaxation components of ^{7}Li in $Li_{0.1}MoS_2$ [d-eth]$_{0.2}$. The inset shows the nonexponential magnetization recovery curve measured at 253 K.

^{7}Li Relaxation. Lithium spin−lattice relaxation times of $Li_{0.1}MoS_2$[d-eth]$_{0.2}$, measured in the temperature range 190−350 K, are displayed in Figure 5. At high temperatures, $T >$ 320 K, the magnetization recovery curve was adequately described by

a single-exponential function for over two time decades. At lower temperatures, $T < 320$ K, the magnetization recovery curves were more adequately fitted by a sum of two exponential functions associated with two different characteristic times, T_{1a} and T_{1b}, of rather different magnitudes. The inset of Figure 5 shows the magnetization recovery curve at 253 K, where one can observe such evident nonexponential behavior. In the temperature range 190−320 K, the amplitude of the fast relaxation decay is more than 50% greater than that of the slow one. The slow component, within experimental error, was found to be relatively temperature-independent, with a relaxation time of $T_{1b} = 4 \pm 1$ s. The fast relaxation time, T_{1a}, shows a more accentuated temperature dependence.

Considering the temperature dependence of both T_{1a} and T_{1b}, we attribute the observation of two ^{7}Li relaxation times in the $Li_{0.1}MoS_2$[d-eth]$_{0.2}$ nanocomposite to the coexistence of two lithium ions with different mobilities. The fast relaxation component, associated with the highly mobile lithium ions, reaches the relaxation rate maximum at $T_{max} \approx 245$ K. It should be noticed that, in lithium ionic conductors and polymer electrolytes, the ^{7}Li relaxation rate maximum is mostly observed above 300 K when measurements are performed at 155 MHz.[41,42] In our case, the observed smaller value of T_{max} indicates that the lithium mobility is high when compared to that of other compounds. We will turn to this point later. However, the slower component, T_{1b}, does not show a clear relaxation rate peak and can be associated with the less-mobile lithium ions, which are probably not clustered in a specific structure but are homogeneously dispersed in the interlaminar space of the nanocomposite.

The longitudinal magnetization recovery of a quadrupolar nucleus, with a single quadrupolar coupling constant, can be described by the sum of two exponential functions with equal amplitude factors.[43] Theoretical predictions and experimental results show that, in this case, the two time constants must have the same temperature dependence. As shown in Figure 5, these conditions are not verified in the case of the magnetization recovery measured in $Li_{0.1}MoS_2$[d-eth]$_{0.2}$, where the amplitude factors associated with the slow and fast exponential contributions differ by 1 order of magnitude, and besides, the temperature dependencies of the time constants are different. These facts support the interpretation of T_{1a} and T_{1b} as the time constants characterizing the magnetization recovery of two kinds of Li sites instead of describing a nonexponential recovery from a unique site.

The nominal lithium/amine ratio of the studied compound is approximately 1:2, and by recalling that the same stoichiometry was used for modeling the Li_3−amine aggregate, we may conclude that the number of lithium ions dispersed in the material (i.e., not belonging to the Li_3 cluster) is very small. Nevertheless, the existence of a small number of dispersed lithium nuclei in the van der Waals gaps can be taken into account to explain both the two observed branches in the relaxation data of Figure 5 and the asymmetry of the low-temperature line shape of Figure 2c. Charge transfer between dispersed lithium ions and the host could promote the formation of paramagnetic centers, and this could be an explanation for the stronger EPR signal observed for the sample with $x = 0.7$, which has a larger lithium/amine ratio. However, the relationship between lithium content and EPR signal intensities is still an open question.

The ^{7}Li NMR relaxation in ionic solids is mainly governed by two mechanisms: (i) quadrupolar relaxation due to the interaction between the quadrupole moment of the ^{7}Li nuclei and the fluctuating electric field gradient produced by the surrounding electrical charge distribution and (ii) the dipolar relaxation produced by random fluctuations of the lithium homo- and heteronuclear dipole−dipole interactions.[16,33,36] Furthermore, paramagnetic centers, impurities, or conduction electrons can contribute to the ^{7}Li line width and provide effective additional relaxation mechanisms.[44,45] Hyperfine interactions between nuclei and conduction electrons can be excluded from our analysis because of the absence of any shift of the ^{7}Li MAS NMR line with respect to $LiCl/H_2O$. If the electrons and nuclear spins occupy fixed positions in space, two combined mechanisms are suggested to explain the nuclear relaxation caused by electron−nuclear couplings: electron relaxation and spin diffusion.[33] If the paramagnetic centers participating in the nuclear relaxation are those responsible for the observed EPR signal, their concentration can be estimated to be very small ($<10^{13}$ spins/cm^3). Within the framework of the proposed model for the Li_3−amine clusters, it is evident that the coupling between Li nuclei and electron spins must be established by magnetic dipolar interactions. Also, considering that the dipolar Li−Li coupling between nuclei belonging to different clusters is negligible, the existence of a spin-diffusion mechanism that will transmit the information on the lattice temperature dispensed by the electronic spins to the remote nuclear spins is very unlikely. Such a diffusion mechanism should occur through the mutual flips between neighboring nuclear spins in the van der Waals gap, transporting their magnetization to the paramagnetic centers in the host. The low concentration of paramagnetic centers and the lack of communication between lithium ions of different clusters should make spin diffusion an inefficient relaxation mechanism.

Because no large shifts of the NMR lines were observed, we might conclude that the ^{7}Li relaxation is not sensitive to the presence of paramagnetic centers (or impurities). Nevertheless, this conclusion is only partially correct because of the following arguments. Let us suppose that a fraction of the lithium nuclei are located near the paramagnetic centers and that they are strongly coupled to their electronic spins. Under such strong coupling conditions, these nuclei would experience a fast spin−lattice relaxation, and as a consequence, they would be unobservable under the current experimental conditions. However, the observed lithium nuclei, clustered in the amine cages, could be coupled to the fast-relaxing nuclei, and as a consequence of such (weak) coupling, additional spin−lattice relaxation routes for the spin magnetization of the clustered nuclei could be established. In a first analysis, the existence of such relaxation processes cannot be discarded, and to quantify their relative importance to the analysis of the present data, more experimental and theoretical work would be necessary. Because our experimental data do not show any clear features that evidence the above hypothesis, it is our intention to consider the fluctuations of the quadrupolar interaction as the main nuclear relaxation path for the clustered lithium ions.

An estimate of the dipolar contribution to the spin−lattice relaxation rate, $(T_1^{-1})_d$, can be obtained from the lithium second moment by using the expression $(T_1^{-1})_d \approx C\gamma^2 M_2/\omega_o$, where ω_o is the ^{7}Li Larmor frequency and C is a constant on the order of unity. Considering the line width of the central line (8.5 kHz) measured without ^{1}H decoupling, the corresponding second moment is M_2(Li) ≈ 4.8 G^2, leading to the result $(T_1^{-1})_d$ on the order of 0.5 s^{-1}. This result is more than 1 order of magnitude smaller than the experimentally measured relaxation value at the rate maximum, $T_1^{-1} \approx 13$ s^{-1} (Figure 5). A more accurate value for $(T_1^{-1})_d$ can be calculated by using a rigorous approach

that makes both homo- and heteronuclear interactions explicit. However, such a procedure is unnecessary because it will give a correction to the calculated $(T_1^{-1})_d$ value. Because the ^{7}Li relaxation rate results from both dipolar and quadrupolar contributions $(T_1^{-1} = (T_1^{-1})_d + (T_1^{-1})_q)$, the quadrupolar contribution is estimated to be $(T_1^{-1})_q \approx 12.5\ s^{-1}$. Therefore, fluctuations of the quadrupolar interaction due to the Li^+ motions are responsible for the spin−lattice relaxation of the ^{7}Li nuclei in $Li_{0.1}MoS_2$[d-eth]$_{0.2}$. For a $I = {}^3/_2$ nuclei, the frequency dependence of $(T_1^{-1})_q$ is given by[33]

$$\left(\frac{1}{T_1}\right)_q = \frac{3\pi^2}{10}\frac{2I+3}{I^2(2I-1)}\left(1+\frac{\eta^2}{3}\right)\left(\frac{e^2qQ}{\hbar}\right)^2\frac{1}{\omega_o}f(\omega_o\tau) \approx \frac{2\pi^2}{5}\left(\frac{e^2qQ}{\hbar}\right)^2\frac{1}{\omega_o}f(\omega_o\tau) \quad (1)$$

The spectral density function

$$f(\omega_o\tau) = \frac{\omega_o\tau}{1+(\omega_o\tau)^2} + \frac{4\omega_o\tau}{1+4(\omega_o\tau)^2} \quad (2)$$

has a maximum at $\omega_o\tau = 0.62$, where $f(0.62) = 1.425$, and is parametrized by the correlation time τ of the molecular motion modulating the nuclear spin interactions. Equation 1 can be expressed as a function of temperature by assuming that a thermally activated process rules motion, as suggested by the T_1^{-1} peak in Figure 5. In this case, an Arrhenius temperature dependence for τ is often assumed: $\tau = \tau_o \exp(E_A/k_BT)$, where k_B is the Boltzmann constant and E_A is the activation energy. The attempt frequency τ_o^{-1} can be interpreted as a vibrational frequency on the order of an optical phonon frequency (10^{12}−$10^{13}\ s^{-1}$). The asymmetry parameter η of the electric field gradient tensor varies from 0 to 1. A maximum error of ∼15% is introduced into the calculation of the coupling constant when η is set equal to 0, as on the right side of eq 1. From the estimated quadrupolar relaxation rate maximum, $(T_1^{-1})_q$, the quadrupole coupling constant is calculated to be $e^2qQ/\hbar \approx 48$ kHz, leading to a theoretical satellite separation of $\nu_q = e^2qQ/2\hbar \approx 24$ kHz, which is comparable to the value obtained for the measured width of the broad baseline, 30 kHz. The value estimated for $e^2qQ/\hbar$ is in agreement with the ^{7}Li quadrupole coupling measured for lithium in other disulfide-layered compounds and transition-metal dichalcogenides, which usually lies in the range 30−50 kHz.[16,46,47]

The activation energy, calculated from the linear slope of the ^{7}Li T_1^{-1} curve on the high-temperature side of the relaxation maximum yields $E_A = 0.18$ eV. This result is in good agreement with the values reported for layered compounds and transition-metal dichalcogenides studied by ^{7}Li NMR, which lie in the range 0.1−0.3 eV.[48−53] From the condition for the maximum relaxation rate, a value of $\tau \approx 10^{-9}$ s is obtained at 245 K, leading to $\tau_o \approx 2 \times 10^{-13}$ s. The attempt frequency τ_o^{-1} can be related to the oscillation frequency, f, of a lithium ion in a potential well, modeled by a sinusoidal barrier shape of energy U_o between wells separated by a distance d[54]

$$f = \frac{1}{d}\sqrt{\frac{U_o}{2m}} \quad (3)$$

where m is the lithium mass. The attempt frequency is equal to the oscillation frequency times the number of possible jumps, which is just one in the case of the Li_3 cluster. Assuming that d is equal to the Li−Li distance in the Li_3 cluster (i.e., $d \approx 2.8$ Å) and that the barrier energy is equal to the lithium motional activation energy ($U_o = 0.18$ eV), eq 3 yields $f \approx 4 \times 10^{12}\ s^{-1}$. This result is in good agreement with the attempt frequency, $\tau_o^{-1} \approx 5 \times 10^{12}\ s^{-1}$, obtained from the relaxation measurements.

The correlation time at 300 K of the lithium motion in the $Li_{0.1}$ MoS_2[d-eth]$_{0.2}$ nanocomposite, $\tau \approx 2 \times 10^{-10}$ s, is at least 1 order of magnitude smaller than those obtained in other lithium intercalation compounds or in fast lithium ionic conductors at the same temperature, which lie between 2×10^{-8} and 5×10^{-9} s.[16,35,53,55,56] Very short correlation times are typical of a fast exchange process. Recently, a ^{7}Li NMR study on the solid tetrameric form of *tert*-butyllithium, where the lithium atoms are rapidly exchanging between the four equivalent apical sites of a tetrahedron with an exchange rate of $\kappa = 1/(4\tau) = 8.5 \times 10^8\ s^{-1}$, was reported.[57] In the nanocomposite $Li_{0.1}MoS_2$[d-eth]$_{0.2}$, the analysis of the ^{7}Li relaxation results indicate that the lithium atoms are undergoing a fast exchange between the three lithium sites in the Li_3−aggregate, with an exchange rate of $\kappa = 1/(3\tau) = 2 \times 10^9\ s^{-1}$ that compares favorably with the value found in *tert*-butyllithium. A fast exchange mechanism, consisting of rotations of the Li_3 aggregate in 120° steps, could exchange lithium atoms among similar coordination environments, giving rise to the exchange-rate value observed experimentally. Under such a hypothesis, the local lithium mobility in our sample should be high compared to the mobility caused by diffusive motional processes.

One question that may arise is related to the apparent C_3 symmetry of the Li_3 aggregate, which should lead to a suppression of the quadrupolar fluctuations. However, the equivalence of the three lithium sites cannot be assumed because the amine cages may be energetically stable in a variety of configurations with ill-defined symmetry. Despite the C_3 symmetry of the Li_3 cluster, the Li_3−amine aggregate has distorted C_3 symmetry, and consequently, the electric field gradient at the three vertexes of the Li_3 cluster may assume different values.

A second question is related to the shape of the relaxation curve of the fast-relaxing component in Figure 5, which is associated with the highly mobile lithium ions. That relaxation maximum is not symmetric, in contrast to the prediction of the Bloembergen, Purcell, and Pound (BPP) model (eq 2). This fact is confirmed by the values of the activation energies, $E^{HT} = 0.18 \pm 0.02$ eV and $E^{LT} = 0.11 \pm 0.04$ eV, extracted from the high- and low-temperatures sides of the relaxation curve, respectively. Deviations from the BPP model are frequently found in nuclear relaxation studies.[36,58] The BPP theory, which assumes random motion and dynamically equivalent environments for all ionic or molecular entities, describes only simple processes (rotation or diffusion). In many condensed-matter systems, these assumptions may no longer be valid because of nonrandom motion or low-dimensionality effects or even when the transport involves microscopic processes possessing no characteristic time scale.[36] The relaxation model for 2D motions predicts that $E^{HT} < E^{LT}$; therefore, our results seem not to be related to low dimensionality effects. Indeed, despite the 2D nature of the van der Waals gap, the spin relaxation induced by the exchange motion of the lithium ions in the Li_3 cluster is characteristic of the local rotation of the molecular group in the aggregate, which is well characterized by the BPP theory. The 2D confinement is a determinant of the self-assembling of the intercalated structures but, in a first approximation, does not affect the local properties of the Li_3 clusters dynamics. Asymmetric relaxation maxima are typical for the ion-motion-induced nuclear-spin relaxation observed in strongly disordered systems, and it is often attributed to a broad distribution of correlation times. In previous work, we were able to trace the

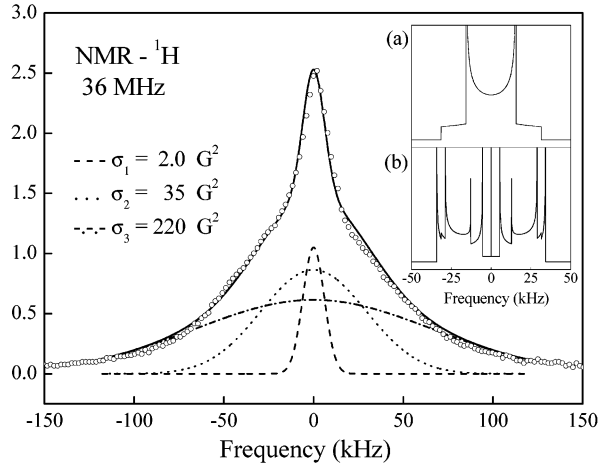

Figure 6. Experimental (○) and simulated (—) ^{1}H NMR spectra at 110 K. Powder line shapes for an isolated pair of nuclei (CH_2) and for three nuclei placed at the corners of an equilateral triangle (CH_3) are shown in insets a and b, respectively. H−H distances within each group are assumed to be 1.8 Å. Intra- and intermolecular interactions of diethylamine ($CH_3-CH_2-NH-CH_2-CH_3$) are taken into account by the convolution of powder line shapes with a Gaussian distribution of the second moment, σ. Convolution results are shown for CH_3 (-.-, $\sigma_3 \approx 176$ G^2) and CH_2 (•••, $\sigma_2 \approx 35$ G^2) groups. The central Gaussian line (- - -, $\sigma_1 \approx 2$ G^2) is associated with the NH group. Relative spectral intensities are 1:4:6 for NH/CH_2/CH_3. Values of the second moments σ_1, σ_2, and σ_3 were chosen to get the best fitting.

origin of this asymmetry to a fast decay of the spin correlation function for times that are short on the scale of the ionic hopping rate, a behavior that seems to be characteristic of highly disordered systems.[59] Electron−nuclear interactions also have to be considered in order to explain the observed asymmetric relaxation maximum. As a matter of fact, nuclear relaxation via paramagnetic centers may have a strong effect on the slope of the low-temperature side of the relaxation maximum, similar to what was observed in our measurement.[60] However, the available data for the low-temperature side of the maximum is insufficient to reach a conclusion in this matter.

The evaluation of $(T_1^{-1})_d$ using the lithium second moment is not necessarily correct in the case where two or more lithium nuclei of different mobilities (different characteristic frequencies) contribute to the ^{7}Li NMR line shape. This question (i.e., whether fluctuations of the quadrupolar interaction may present a dominant mechanism for the ^{7}Li relaxation in the present study) can be answered when comparing the relaxation times of ^{6}Li and ^{7}Li. The ^{6}Li quadrupolar moment is 60 times smaller than the ^{7}Li moment; therefore, $T_1(^6\text{Li})$ should be nearly 3000 times longer than $T_1(^7\text{Li})$ in the case of quadrupolar relaxation.[44] Such an experiment could also provide some insight into the importance of the contribution of the electronic spins to the ^{7}Li relaxation. However, partially because of the low concentration of lithium in our sample and the intrinsic low sensitivity associated with these nuclei, no ^{6}Li NMR signal was observed. Besides, a much longer T_1 value with respect to that of ^{7}Li could also be the reason that we did not observe a ^{6}Li NMR signal in our experiment, and if this was the case, such a result would be in accordance with the attribution of the quadrupolar interaction as the main relaxation mechanism.

^{1}H NMR Spectra. The static ^{1}H NMR spectrum of solid $Li_{0.1}MoS_2$ [d-eth]$_{0.2}$ obtained at 110 K is shown in Figure 6. The observed line shape is slightly asymmetric and can be fitted by a superposition of Gaussian lines. Because of the large number of Gaussian components needed to fit the spectra and the consequent excessive number of self-correlated parameters, an arbitrary fitting procedure may lead to a nonunique interpretation. To give physical meaning to the fitting analysis, one needs to invoke previous knowledge of the material structure. First of all, assuming that the experimental temperature was sufficiently low, it is expected that a relevant broadening source for the observed broad spectrum should be the dipole−dipole interactions between the protons in the rigid-lattice diethylamine cluster. Second, the large number of protons within the cluster and the almost random relative orientations between adjacent molecular groups produce a distribution of local fields, causing the broadening of the spectrum. Third, one usually expects that the intercluster interactions, if present, should be an additional spectral-broadening source.

A more detailed analysis of the spectrum shown in Figure 6 can be performed on the basis of the chemical structure of the diethylamine cluster proposed previously. To simplify the analysis, we recall that the cluster is constituted by the chemical arrangement of the molecular groups NH, CH_2, and CH_3. The NMR powder spectra of isolated CH_2 and CH_3 groups can be calculated from first principles, and the results, well described in the literature, are reproduced in insets a and b of Figure 6. Powder spectra of inset a, known as a Pake dublet,[33] are attributed to a pair of protons 1.8 Å apart in the CH_2 group. The inset b spectrum is attributed to the CH_3 groups and is calculated from an arrangement of three protons separated by 1.79 Å placed at the corners of an equilateral triangle.[61] Neighboring group interactions broaden the lines and smooth out the discontinuities, resulting in a broadened spectrum. A Gaussian broadening function is a fair approximation to take into account the effect of neighboring group interactions. Usually, the convolution of a Gaussian broadening function, of a moderate second moment, with the isolated group powder spectra results in a partially resolved spectral structure of two (CH_2) or three (CH_3) peaks. Such resolved structure is not observed in our experimental data, suggesting a stronger intergroup interaction that can be represented by a Gaussian broadening function with a larger second moment. Indeed, calculation shows that a reasonable fitting of the experimental data can be achieved by assuming that the NH, CH_2, and CH_3 powder spectra are broadened by Gaussian functions of second moments 2.0, 35, and 220 G^2. The relative integrated intensities of the lines were set as fixed parameters and were equal to 1:4:6, respectively. According to these data, the resulting fitted spectrum has a second moment of 257 G^2.

On the basis of the spatial coordinates of the atoms in the cluster shown in Figure 3, the hydrogen second moment can be calculated from first principles according to the expression[33]

$$M_2(\text{H}-\text{H}) = \frac{9}{20}\gamma_H^2\hbar^2\frac{1}{N}\sum_{j\neq k}^{N}\frac{1}{R_{jk}^6} \qquad (4)$$

where M_2 is expressed in units of G^2, γ_H is the hydrogen magnetogyric ratio, $N = 66$ is the number of hydrogen nuclei in each cluster, and R_{jk} is the distance between hydrogen nuclei j and k. The result obtained from eq 4 gives M_2(H−H) = 60 G^2, which is smaller than the second moment (257 G^2) determined by the fitting procedure. The partial contributions of the NH, CH_2, and CH_3 groups to the total second moment can also be discriminated from eq 4. The result is M_2(NH) = 1.8 G^2, $M_2(CH_2)$ = 19 G^2, and $M_2(CH_3)$ = 39 G^2, which are smaller than the second moments estimated from the fitting by factors 1.1, 1.8, and 5.6, respectively. It is apparent that the discrepancy between the calculated and fitted parameters increases with the proximity of the corresponding hydrogen

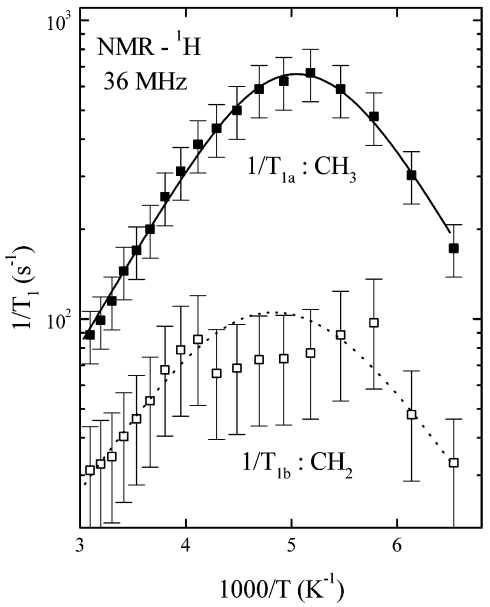

Figure 7. Temperature dependence of the fast (T_{1a}^{-1}) (■) and slow (T_{1b}^{-1}) (□) spin−lattice relaxation components of ^{1}H in $Li_{0.1}MoS_2$ [d-eth]. The solid and dashed lines correspond to the fitting procedure described in the text. The resulting fitted parameters are $E_A = 0.12$ eV and $\tau_o = 2.4 \times 10^{-12}$ s for the CH_3 group (—) and $E_A = 0.10$ eV and $\tau_o = 1.0 \times 10^{-11}$ s for the CH_2 group (- - -).

group to the border of the cluster. This observation can be explained by assuming two facts. First, the intercalation of the molecule imposes a geometrical restriction, causing severe packing and decreasing H−H distances. Second, the fairly high concentration of lithium atoms and diethylamine molecules favors the proximity between clusters, increasing cluster−cluster interactions.

Figure 4 shows the temperature dependence, in the range 93−320 K, of the line width of the central component of the ^{1}H NMR spectrum, which is associated with the hydrogens in the NH group. Only one line-narrowing onset was observed at ∼145 K. The abrupt decrease in line width results in a residual line width that is only a small fraction of the initial low-temperature rigid-lattice value. The motional narrowing of the ^{1}H NMR line begins when the rate of the local magnetic field fluctuations, $1/\tau$, is comparable to the dipolar rigid-lattice line width, $\Delta H_{RL} \approx 15$ kHz. As in the case of ^{7}Li NMR, this condition can be expressed in terms of the second moment of the NH group by $(\gamma\ M_2)^{1/2}\tau \ll 1$. Using $M_2 = 2.2$ G^2 results in $\tau \ll 2.8 \times 10^{-5}$ s.

^{1}H NMR Spin−Lattice Relaxation. The ^{1}H spin−lattice relaxation was found to be nonexponential throughout the investigated temperature range, 150−330 K. The magnetization curves were fitted by a sum of two exponential functions characterized by a short (T_{1a}) and a long (T_{1b}) relaxation time. Figure 7 shows the temperature dependence of T_{1a}^{-1}, whose main feature is the maximum rate observed at ∼200 K. Measurement of the slow-relaxing contribution, T_{1b}^{-1}, is more affected by noise and shows a less-resolved peak also around 200 K. Maximum relaxation rates, measured at 200 K, are 650 and 100 s^{-1} for the fast and slow components, respectively. The relative amplitudes of the fast- and slow-relaxing exponential functions vary with temperature, being about 10:1 below 250 K, decreasing at higher temperatures, and reaching 1:1 at 330 K.

The observed nonexponential relaxation can be attributed to the coexistence of different types of protonic species with different mobilities. From the line shape analysis, three different species are identified, namely, the hydrogen nuclei belonging to the NH, CH_2, and CH_3 groups. Nuclei belonging to the same molecular group should relax exponentially with the same time constant, and if the relaxation time of species i is designed by T_{1i}, the corresponding magnetization recovery is given by $(M_0^i - M_z^i(t))/M_0^i = \exp(-t/T_{1i})$ For all spins relaxing simultaneously, the total magnetization recovery is

$$\psi(t) = \frac{M_o - M_z(t)}{M_o} = \frac{1}{3}\sum_{i=1}^{3}\frac{M_o^{\,i} - M_z^i(t)}{M_o^{\,i}} = \frac{\sum_{i=1}^{3} A_i \exp(-t/T_{1i})}{\sum_{i=1}^{3} A_i} \quad (5)$$

which, in general, is a nonexponential decay.

The proton spin−lattice relaxation of the $[(C_2H_5)_2NH]$ cluster arises primarily from the modulation of the proton−proton dipolar interactions caused by a series of dynamic processes such as reorientational and librational motions of the CH_3 and the CH_2 groups in the diethylamine molecule. The protons in the NH group have more restricted mobility and may also participate in the relaxation process via spin diffusion.[62,63] When the relaxation results from the random rotation of one molecular group, the relaxation rate is given by[33]

$$\left(\frac{1}{T_1}\right)_i = \frac{2}{5}\frac{\gamma^4\hbar^2}{r^6} I(I+1)\frac{f(\omega_o\tau_i)}{\omega_o} = \frac{2}{3}\gamma^2(\Delta M_2^{\,i})^2\frac{f(\omega_o\tau_i)}{\omega_o} \quad (6)$$

where r is the distance between two nuclei and ΔM_2^i is the difference in the line-shape second moment of species i before and after the onset of motional narrowing (also called the reduced second moment).

The line shape and relaxation data can be interpreted by means of the proposed structural model for the diethylamine cluster. The simplest hypothesis is to assume that the fast-relaxing component, T_{1a}^{-1}, is associated with the highly mobile protons of the CH_3 group and that the slow component, T_{1b}^{-1}, arises from the less-mobile CH_2 group. This assignment is supported by the quantitative estimate of the second moments associated with the relative contributions of these molecular groups to the observed line shape. It is clear from the previous discussion that the second moment associated with the NH group is much smaller than the others, hence its contribution to the observed relaxation rate should be neglected. We conclude that only the CH_3 and CH_2 groups contribute to the observed relaxation, being responsible for the fast T_{1a}^{-1} and slow T_{1b}^{-1} relaxation rates, respectively.

If one uses the second moments calculated from the contributions of the CH_2 and CH_3 groups to the line width (i.e., $\Delta M_2 =$ 35 and 220 G^2, respectively), their corresponding relaxation rates can be calculated from eq 6 using as adjustable parameters only E_A and τ_o. The results of such a calculation are plotted in Figure 7 (as solid and dashed lines), assuming $E_A(CH_3) = 0.12$ eV, $E_A(CH_2) = 0.10$ eV, $\tau_o(CH_3) = 2.4 \times 10^{-12}$ s, and $\tau_o(CH_2) = 1.0 \times 10^{-11}$ s. Despite the large scattering of the T_{1b}^{-1} data, it is clear from Figure 7 that a single set of parameters is not sufficient to fit both components of the relaxation data. It is apparent that in the case of the slow component the maximum relaxation rate occurs at a higher temperature, indicating that the CH_2 group has less mobility than the CH_3 group.

An interesting feature of our ^{1}H data is the extremely short relaxation time of $T_{1a} \approx 1.5$ ms observed at 200 K in Figure 7

(i.e., at the relaxation rate maximum). This value is 20 times smaller than the spin−lattice relaxation time observed in methylamonium compounds ($T_1 \approx 30$ ms) measured at a similar Larmor frequency.[25] Indeed, in the methylamonium compounds, the ammonium cations are packed in an ionic crystal that optimizes cation−anion interactions; meanwhile, the methyl groups in our intercalated cluster are located together in a van der Waals packing of the cluster in the 2D interlaminar space. Proton relaxation times on the order of 15 ms are observed in molybdenum disulfide dipentylamine, $Li_{0.1}MoS_2$[d-pn], whereas T_{1a} values in the range of 1.3−6.0 ms are measured in nanocomposites with dicyclohexylamine, $Li_{0.1}MoS_2$[d-c-hex].[64] Short nuclear relaxation times are often interpreted as a consequence of the presence of paramagnetic impurities in the samples, where the mechanism of relaxation is associated with the dipolar coupling between the proton and paramagnetic ions. As shown above, the explanations for the short T_{1a} values observed in Figure 7 are (a) the large proton dipolar second moment caused by the particular arrangement of the diethylamine group in the nanocomposite $Li_{0.1}MoS_2$[d-eth]$_{0.2}$ and possibly (b) the modulation of the H−Li dipolar interaction caused by the fast lithium motion in this nanocomposite.

IV. Conclusions

This paper reports an NMR study of line shapes and relaxation rates of the nanocomposite obtained from the co-intercalation of lithium and diethylamine in molybdenum disulfide, $Li_{0.1}MoS_2$[d-eth]$_{0.2}$. From the study of the NMR properties of both ^{1}H and ^{7}Li nuclei, it was possible to have a comprehensive view of the structural and dynamical properties of lithium and amine in this nanocomposite. The fundamental ideas supporting this work are based on a proposed model for the material structure in which the co-intercalation process leads to the self-assembling of Li_3 clusters stabilized by amine ligands within the interlaminar spaces. The model has the advantage of being consistent with the geometrical restrictions imposed by the available space between host layers as well as explaining most of the relevant NMR results obtained in such a complex system. The present ^{7}Li NMR studies provide strong evidence of the fast-exchange motion of the three clustered lithium atoms between equivalent coordination sites within the aggregate. The structure and dynamics of the guest diethylamine molecule were studied by proton resonance. The high second moment obtained from the ^{1}H line shape and the strong packing of the intercalated material indicate that the hydrogen nuclei belonging to the CH_3 groups are more sensitive to cluster−cluster dipole−dipole interactions. Second-moment parameters determined from the line-shape fittings were used to calculate spin−lattice relaxation rates that are in good agreement with the experimental data. The nonexponential relaxation of the protons indicates that their mobility increases for those nuclei located closer to the border of the cluster.

Acknowledgment. The financial support of FAPESP (Brazil), FONDECYT (Chile) (grants 798 0054 and 198 1082), Fundación Andes (grant C-12510), and DID Universidad de Chile is gratefully acknowledged.

References and Notes

(1) *Solid State Batteries: Materials Design and Optimization;* Julien, C., Nazri, G. A., Eds.; Kluwer Academic: Boston, 1994.

(2) Broussely, M.; Bienson, P.; Simon, B. *Electrochim. Acta* **1999**, *45*, 3−22 (special issue in lithium insertion into host materials).

(3) Benavente, E.; Santa Ana, M. A.; Mendizábal, F.; González, G. *Coord. Chem. Rev.* **2002**, *224*, 87.

(4) Wiegers, G. A. *Prog. Solid State Chem.* **1996**, *24*, 1−139.

(5) Friend, R. H.; Yoffe, A. D. *Adv. Phys.* **1987**, *36*, 1−94.

(6) Yoffe, A. D. *Solid State Ionics* **1990**, *39*, 1.

(7) Kanatzidis, M. G.; Bissessur, R.; Degroot, D. C.; Schindler, J. L.; Kannewurf, C. R. *Chem. Mater.* **1993**, *5*, 595.

(8) Wang, L.; Schindler, J. L.; Thomas, J. A.; Kannewurf, C. R.; Kanatzidis, M. G. *Chem. Mater.* **1995**, *7*, 1753.

(9) Ibrahim, M. A.; Lee, G. B.; Park, N. G.; Pugh, J. R.; Eberl, D. D.; Frank, A. J. *Synth. Met.* **1999**, *105*, 35.

(10) Alexiev, V.; Meyer zu Altenschildesche, H.; Prins, R.; Weber, Th. *Chem. Mater.* **1999**, *11*, 1742.

(11) Ruiz-Hitzky, E.; Jimenez, R.; Casal, Bl.; Manriquez, V.; Santa Ana, A.; González, G. *Adv. Mater. (Weinheim, Ger.)* **1993**, *5*, 738.

(12) González, G.; Santa Ana, M. A.; Benavente, E.; Donoso, J. P.; Bonagamba, T. J.; Mello, N. C.; Panepucci, H. *Solid State Ionics* **1996**, *85*, 225.

(13) Golub, A. S.; Shumilova, I. B.; Novikov, Yu. N., Mansot, J. L.; Danot, M. *Solid State Ionics* **1996**, *91*, 307.

(14) Wein, E.; Müller-Warmuth, W.; Schöllhorn, R. *Solid State Ionics* **1987**, *22*, 231.

(15) Sanches, V.; Benavente, E.; Santa Ana, M. A.; González, G. *Chem. Mater.* **1999**, *11*, 2296.

(16) León, C.; Lucía, M. L.; Santa Maria, J.; París, M. A.; Sanz, J.; Várez, A. *Phys. Rev. B* **1996**, *54*, 1996.

(17) Emery, J.; Bohnke, O.; Fourquet, J. L.; Buzaré, J. Y.; Florian, P.; Massiot, D. *J. Phys.: Condens. Matter* **1999**, *11*, 10401.

(18) Wang, L. Q.; Exarhos, G. J.; Liu, J. *Adv. Mater. (Weinheim, Ger.)* **1999**, *11*, 1331.

(19) Yamauchi, M.; Ishimaru, S.; Ikeda, R. *Z. Naturforsch., A: Phys. Sci.* **1999**, *54*, 755.

(20) Xie, X.; Hayashi, S. *J. Phys. Chem. B* **1999**, *103*, 5956.

(21) Fenrych, J.; Reynhardt, E. C.; Jurga, S.; Jurga, K. *Mol. Phys.* **1993**, *79*, 559.

(22) Wong, S.; Vaia, R. A.; Giannelis, E. P.; Zax, D. B. *Solid State Ionics* **1996**, *86*−*88*, 547.

(23) Yang, D. K.; Zax, D. B. *J. Chem. Phys.* **1999**, *110*, 5325.

(24) Jacobs, D. M.; Zeidler, M. D.; Kanert, O. *J. Phys. Chem. A* **1997**, *101*, 5241.

(25) Jagadeesh, B.; Rajan, P. K.; Venu, K.; Sastry, V. S. S. *Solid State Commun.* **1993**, *86*, 803. Jagadeesh, B.; Rajan, P. K.; Venu, K.; Sastry, V. S. S. *J. Phys. Chem. Solids* **1993**, *54*, 527.

(26) Murthy, B. V. S.; Ramesh, K. P.; Ramakrishna, J. *J. Phys. Chem. Solids* **2000**, *61*, 961.

(27) Dines, M. B. *Mater. Res. Bull.* **1975**, *10*, 287.

(28) Benavente, E.; González, G. *Mater. Res. Bull.* **1997**, *32*, 709.

(29) González, G.; Binder, H. *Bol. Soc. Chil. Quím.* **1996**, *41*, 121.

(30) Bensimon, Y.; Belougne, P.; Deroide, P.; Zanchetta, J. V.; Giuntini, J. C.; Henn, F. *J. Non-Cryst. Solids* **1992**, *149*, 218−228.

(31) Kunwar, A. C.; Turner, G. L.; Oldfield, E. *J. Magn. Reson.* **1986**, *69*, 124.

(32) *ACD/CNMR*, version 1.1; Advanced Chemistry-Development Inc.: Toronto, Ontario/Canada, 1994/1995.

(33) Abragam, A. *Principles of Nuclear Magnetism;* Oxford University: London, 1961.

(34) Stallworth, P. E.; Kostov, S.; denBoer, M. L.; Greenbaum, S. G.; Lampe-Onnerud, C. *J. Appl. Phys.* **1998**, *83*, 1247.

(35) Guedes, F. B. M.Sc. Thesis, IFSC, University of São Paulo, São Paulo, Brazil, 1997.

(36) Donoso, J. P.; Bonagamba, T. J.; Panepucci, H. C.; Oliveira, L. N.; Gorecki, W.; Berthier, C.; Armand, M. *J. Chem. Phys.* **1993**, *98*, 10026.

(37) Donoso, J. P.; Bonagamba, T. J.; Frare, P. L.; Mello, N. C.; Panepucci, H. C. *Electrochim. Acta* **1995**, *40*, 2361.

(38) Gonzalez-Moraga, G. *Cluster Chemistry*; Springer-Verlag: Berlin, 1993.

(39) Weiss, E.; Henchen, G. *J. Organomet. Chem.* **1970**, *21*, 265.

(40) Köster, H.; Thoennes, D.; Weiss, E. *J. Organomet. Chem.* **1978**, *160*, 1.

(41) Bechtold-Schweckert, E.; Mali, M.; Roos, J.; Brinkmann, D. *Phys. Rev. B* **1984**, *30*, 2891.

(42) Bader, B.; Heitjans, P.; Stockmann, H. J.; Ackermann, H.; Buttler, W.; Freiländer, P.; Kiese, G.; Van der Marel, C.; Schirmer, A. *J. Phys.: Condens. Matter* **1992**, *4*, 4779.

(43) Bonera, G.; Borsa, F.; Rigamonti, A. *Phys. Rev. B* **1970**, *2*, 2784.

(44) Pietrass, T.; Taulelle, F.; Lavela, P.; Olivier-Fourcade, J.; Jumas, J.; Steuernagel, S. *J. Phys. Chem. B* **1997**, *101*, 6715.

(45) Winter, R.; Heitjans, P. *J. Phys. Chem. B* **2001**, *105*, 6108.

(46) Silbernagel, B. G. *Solid State Commun.* **1975**, *17*, 361.

(47) Prigge, C.; Muller-Warmuth, W.; Gocke, E.; Schollhorn, R. *Z. Phys. Chem.* **1995**, *189*, 153.

(48) Asai, T.; Sugimoto, S.; Kawai, S.; Okada, Sh.; Yamaki, J. *Mater. Res. Bull.* **1989**, *24*, 75.

(49) Cocciantelli, J. M.; Suh, K. S.; Senegas, J.; Doumerc, J. P.; Soubeyroux, J.; Pouchard, M.; Hagenmuller, P. *J. Phys. Chem. Solids* **1992**, *53*, 51.

(50) Wang, G.; Roos, J.; Brinckmann, D.; Pasquali, M.; Pistoia, G. *J. Phys. Chem. Solids* **1993**, *54*, 851.

(51) León, C.; Santa Maria, J.; París, M. A.; Sanz, J.; Ibarra, J.; Várez, A. *J. Non-Cryst. Solids* **1998**, *235*−*237*, 753.

(52) Matsumoto, K.; Nagai, R.; Asai, T.; Kawai, S. *Solid State Ionics* **1987**, *25*, 233.

(53) Kuchler, W.; Heitjans, P.; Payer, A.; Schollhorn, R. *Solid State Ionics* **1994**, *70*−*71*, 434.

(54) Bohnke, O.; Emery, J.; Veron, A.; Fourquet, J. L.; Buzare, J. Y.; Florian, P.; Massiot, D. *Solid State Ionics* **1998**, *109*, 25.

(55) Bertermann, R.; Muller-Warmuth, W.; Jansen, C.; Hiltmann, F.; Krebs, B. *Solid State Ionics* **1999**, *117*, 245.

(56) Grüne, M.; Müller-Warmuth, W.; Hebel, P.; Krebs, B. *Solid State Ionics* **1993**, *66*, 165.

(57) Vanhoorne, P.; Grandjean, J.; Jérôme, R. *Macromolecules* **1995**, *28*, 3553.

(58) Brinkmann, D. *Magn. Reson. Rev*. **1989**, *14*, 101.

(59) Donoso, J. P.; Oliveira, L. N.; Panepucci, H.; Cassanho, A.; Guggenheim, H. *J. Phys. C: Solid State Phys.* **1986**, *19*, 963.

(60) Bork, D.; Heitjans, P. *J. Phys. Chem. B* **2001**, *105*, 9162.

(61) Andrew, E. R.; Bersohn, R. *J. Chem. Phys*. **1950**, *18*, 159.

(62) Idziak, S.; Jakubas, R. *Solid State Commun.* **1987**, *62*, 173.

(63) Tritt-Goc, J.; Pislewski, N.; Pawlowski, A.; Goc, R. *Solid State Commun.* **1998**, *106*, 367.

(64) Bloise, A. C. Unpublished results.